BIOCHEMISTRY
including biophysical chemistry & molecular biology
Article

Biochemistry **2009,** *48,* 6191–6201 6191
DOI: 10.1021/bi900629e

Structural Basis for the Sugar Nucleotide and Acyl-Chain Selectivity of *Leptospira interrogans* LpxA†

Lori I. Robins,‡ Allison H. Williams,‡ and Christian R. H. Raetz*

Department of Biochemistry, Duke University Medical Center, Box 3711, Durham, North Carolina 27710 ‡*Both authors contributed equally to this work*

Received April 12, 2009; Revised Manuscript Received May 19, 2009

ABSTRACT: The first step of lipid A biosynthesis is catalyzed by LpxA in *Escherichia coli* (EcLpxA), an acyltransferase selective for UDP-GlcNAc and *R*-3-hydroxymyristoyl-acyl carrier protein (ACP). *Leptospira interrogans* LpxA (LiLpxA) is extremely selective for *R*-3-hydroxylauroyl-ACP and an analogue of UDP-GlcNAc, designated UDP-GlcNAc3N, in which NH_2 replaces the GlcNAc 3-OH group. EcLpxA does not discriminate between UDP-GlcNAc and UDP-GlcNAc3N; however, *E. coli* does not make UDP-GlcNAc3N. With LiLpxA, *R*-3-hydroxylauroyl-methylphosphopantetheine efficiently substitutes for *R*-3-hydroxylauroyl-ACP. We now present crystal structures of free LiLpxA and its complexes with its product UDP-3-*N*-(*R*-3-hydroxylauroyl)-GlcNAc3N and with its substrate *R*-3-hydroxylauroyl-methylphosphopantetheine. The positions of the acyl chains of the *R*-3-hydroxylauroyl-methylphosphopantetheine and the UDP-3-*N*-(*R*-3-hydroxylauroyl)-GlcNAc3N are almost identical and are similar to that of the acyl chain in the EcLpxA/UDP-3-*O*-(*R*-3-hydroxymyristoyl)-GlcNAc complex. The selectivity of LiLpxA for UDP-GlcNAc3N may be explained by the orientation of the backbone carbonyl group of Q68, which differs by ~82° from the corresponding Q73 carbonyl group in EcLpxA. This arrangement provides an extra hydrogen-bond acceptor for the 3-NH_2 group of UDP-GlcNAc3N in LiLpxA. The *R*-3-hydroxylauroyl selectivity of LiLpxA is explained by the position of the K171 side chain, which limits the length of the acyl-chain-binding groove. Our results support the role of LiLpxA H120 (which corresponds to EcLpxA H125) as the catalytic base and provide the first structural information about the orientation of the phosphopantetheine moiety during LpxA catalysis.

Leptospira interrogans, a spirochete that inhabits areas with warm, humid climates, thrives in fresh water sources contaminated by animal urine (*1*). *L. interrogans* infect humans who come in contact with the contaminated water or soils, causing Weil's disease, which damages the liver, kidneys, heart, and lungs (*1*) and may be fatal if left untreated (*2*). *L. interrogans* is a spirochete that is able to survive outside of its host and one of the few that synthesizes lipopolysaccharide (LPS)[1] (*3*, *4*). Accordingly, all *L. interrogans* genomes encode orthologues of the *Escherichia coli* Lpx enzymes (*3*, *4*), which are responsible for the assembly of the Kdo_2-lipid A anchor of LPS (Figure 1).

Some Gram-negative bacteria, including *L. interrogans*, synthesize variants of lipid A, in which a 2,3-diamino-2,3-dideoxy-D-glucopyranose (GlcN3N) unit replaces one or both glucosamine residues (*5*, *6*). *L. interrogans* lipid A contains two such GlcN3N units (*6*) (Figure 1A). The GlcN3N residues are derived from UDP-2-acetamido-3-amino-2,3-dideoxy-α-D-glucopyranose (UDP-GlcNAc3N) (Figure 1A) (*7*, *8*). This material is synthesized from UDP-GlcNAc by the sequential actions of the dehydrogenase GnnA and the transaminase GnnB; these proteins are not present in *E. coli* (Figure 1A) (*7*, *8*).

L. interrogans LpxA (LiLpxA) transfers the *R*-3-hydroxylauroyl chain from *R*-3-hydroxylauroyl-ACP to UDP-GlcNAc3N (*6*, *7*) (Figure 1A). LiLpxA shows an absolute selectivity for UDP-GlcNAc3N (Figure 1A) (*7*). EcLpxA acylates both UDP-GlcNAc and UDP-GlcNAc3N *in vitro* with equal efficiency (*7*) (not shown in Figure 1A), but UDP-GlcNAc3N is not synthesized by wild-type *E. coli*. LiLpxA also shows a striking preference for *R*-3-hydroxylauroyl-ACP over other hydroxyacyl-ACPs (*7*) (Figure 1A). *E. coli* LpxA (EcLpxA) is highly selective for *R*-3-hydroxymyristoyl-ACP (Figure 1B), but it can also slowly use *R*-3-hydroxylauroyl- and *R*-3-hydroxypalmitoyl-ACP (*7*, *9*, *10*).

Initial biochemical studies of EcLpxA suggested a mechanism in which H125 is the catalytic base (*11*) (Scheme 1). Recent structural studies have confirmed that the NE2 atom of H125 is within hydrogen-bonding distance of the 3-OH group of the glucosamine ring in complexes of EcLpxA with

*To whom correspondence should be addressed. Telephone: (919) 684-5326. Fax: (919) 684-8885. E-mail: raetz@biochem.duke.edu.

†This research was supported by National Institutes of Health (NIH) Grant GM-51310 to C.R.H.R. A.H.W. was supported by the Cellular and Molecular Biology Training Grant GM-07184 to Duke University.

[1]Abbreviations: ACP, acyl carrier protein; EcLpxA, *Escherichia coli* UDP-GlcNAc acyltransferase; GlcN3N, 2,3-diamino-2,3-dideoxy-D-glucopyranose; LiLpxA, *Leptospira interrogans* UDP-GlcNAc3N acyltransferase; LPS, lipopolysaccharide; UDP-GlcNAc, UDP-*N*-acetylglucosamine; UDP-GlcNAc3N, UDP-2-acetamido-3-amino-2,3-dideoxy-α-D-glucopyranose.

Published on Web 05/20/2009

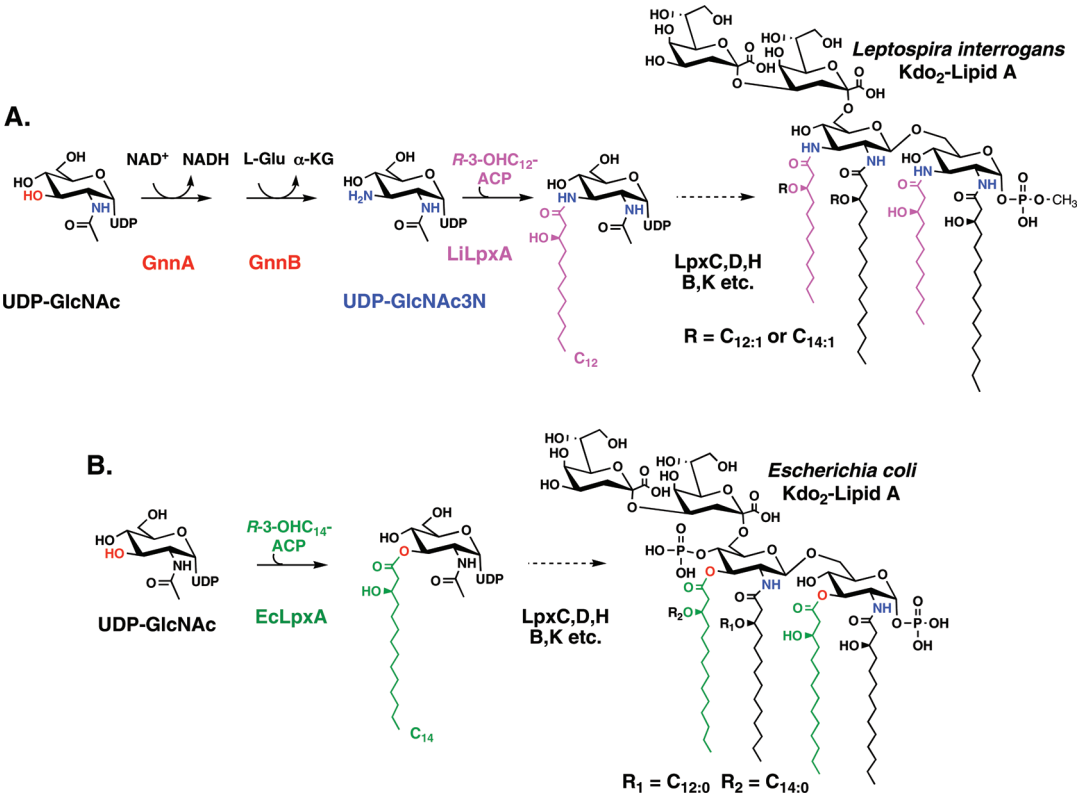

FIGURE 1: Substrate selectivity of LiLpxA versus EcLpxA and the origin of UDP-GlcNAc3N. (A) Biosynthesis of UDP-GlcNAc3N, substrate selectivity of LiLpxA, and structure of *L. interrogans* lipid A (*6*−*8*). The *R*-3-hydroxylauroyl (*R*-3-OHC$_{12}$) chain is shown in magenta in both the LiLpxA product and the lipid A generated by *L. interrogans*. (B) Selectivity of EcLpxA and structure of *E. coli* lipid A (*12*). The *R*-3-hydroxymyristate (*R*-3-OHC$_{14}$) chain is shown in green. The *E. coli* chromosome does not encode GnnA and GnnB, but EcLpxA can use UDP-GlcNAc3N as efficiently as UDP-GlcNAc *in vitro* (*7*).

UDP-GlcNAc (*12*). These structures also elucidated the roles of the conserved EcLpxA residues Q73, L75, H99, H122, H144, Q161, N198, and R205 in substrate binding (Scheme 1) (*12*). The NH group of G143 is the proposed oxyanion hole (Scheme 1). The preference of EcLpxA for *R*-3-hydroxymyristoyl-ACP is explained by the positioning of G173 and H191 (*12*). The reaction catalyzed by EcLpxA with UDP-GlcNAc is reversible and thermodynamically unfavorable in the forward direction (*11*, *13*).

The structure of a LpxA orthologue selective for UDP-GlcNAc3N has not been investigated. Herein, we report the crystal structures of LiLpxA in the free form at 2.10 Å, with bound UDP-3-*N*-(*R*-3-hydroxylauroyl)-GlcNAc3N at 2.10 Å and with bound *R*-3-hydroxylauroyl-methylphosphopantetheine at 2.12 Å. The latter compound is an effective model substrate for LiLpxA but not EcLpxA. The space group is trigonal (*P*321). The asymmetric unit of LiLpxA contains three protein molecules, whereas that of EcLpxA contains only one (*12*, *14*). However, the active-site cleft of the biologically relevant LiLpxA homotrimer (which is not the same as three monomers in the asymmetric unit) is similar to that of EcLpxA (*12*), and its structure explains the *R*-3-hydroxylauroyl-ACP selectivity of LiLpxA. The altered position of the backbone carbonyl moiety of Q68 in LiLpxA provides a favorable hydrogen-bond acceptor for the NH_2 moiety of UDP-GlcNAc3N but discriminates against the 3-OH group of UDP-GlcNAc. The UDP-GlcNAc3N selectivity of LiLpxA is reminiscent of the mechanism of bacterial resistance to vancomycin.

MATERIALS AND METHODS

Materials. Unless otherwise noted, chemicals and chromatography supplies were purchased from VWR Scientific (West Chester, PA). Ampicillin, kanamycin, NAD, pyridoxine, and α-ketoglutarate were purchased from Sigma-Aldrich (St. Louis, MO). [α-^{32}P]-UTP was from Perkin-Elmer (Waltham, MA). *R*-3-Hydroxylauroyl-methylphosphopantetheine was synthesized by Avanti Polar Lipids (Alabaster, AL). PEG 3350 and diammonium citrate crystallography solutions were purchased from Hampton Research (Aliso Viejo, CA). Plasmids were purified using a Qiaprep miniprep spin column kit (Qiagen, Valencia, CA).

Overexpression and Purification of LiLpxA. The hybrid plasmid pLP3 (*7*), which overexpresses LiLpxA from the T7 promoter of pET30a(+), was transformed into *E. coli* BL21 (DE3)/pLysS (Stratagene, La Jolla, CA). Cells were grown at 37 °C in 1 L of LB medium (*15*, *16*) with kanamycin (30 μg/mL), induced with 1 mM isopropyl-β-D-thiogalactopyranoside (IPTG) at A_{600} = 0.6, and grown for an additional 3 h. The cells were harvested by centrifugation at 4000*g* and washed with 100 mL of 10 mM potassium phosphate at pH 7.0 containing 200 mM NaCl and 20% glycerol. The cell pellet was resuspended in 20 mL of the same buffer and frozen at −80 °C. Cells were lysed by two passages through a French pressure cell at 16 000 psi. Cell debris was removed by centrifugation at 10000*g* for 30 min. Ultracentrifugation at 150000*g* for 1 h provided a membrane-free lysate. Successful overexpression of LiLpxA was confirmed by sodium dodecyl sulfate−polyacrylamide gel electrophoresis (SDS−PAGE). The membrane-free lysate (20 mL) was then loaded onto a 50 mL Green-19 column (Sigma-Aldrich, St. Louis, MO) at 1.5 mL/min. The column was washed with three volumes of 10 mM potassium phosphate at pH 7.0 containing 200 mM NaCl and 20% glycerol (v/v). Next, the column was washed with three volumes of 10 mM potassium phosphate at pH 7.0 containing

Scheme 1: Proposed Catalytic Mechanism of EcLpxA and Roles of Key Residues in Substrate Binding

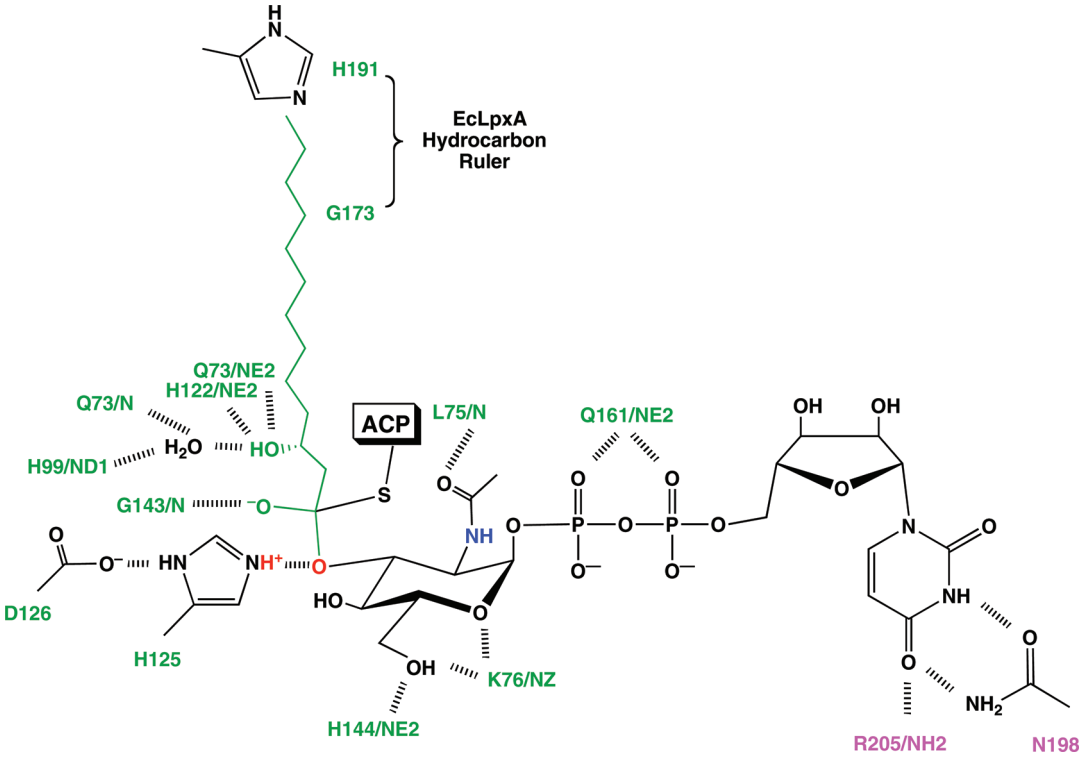

600 mM NaCl and 20% glycerol. LiLpxA was eluted with 500 mL of 10 mM potassium phosphate at pH 7.0 containing 1.5 M NaCl and 20% glycerol. The fractions (~10 mL each) containing LiLpxA were pooled, dialyzed into 20 mM Tris chloride buffer at pH 8.0 containing 20% glycerol, and loaded onto a 10 mL Source 30Q (GE Healthcare, Chalfont, St. Giles, U.K.) ion-exchange column, equilibrated with the same buffer. A 200 mL gradient from 0 to 1 M NaCl was applied; the LiLpxA eluted between 200 and 300 mM NaCl. Fractions (4 mL each) containing LiLpxA were concentrated to 10 mg/mL, and 5 mL portions were loaded onto a Superdex 200 gel filtration column (330 mL, GE Healthcare, Chalfont, St. Giles, U.K., equilibrated in 10 mM Tris chloride at pH 8.0 containing 250 mM NaCl and 20% glycerol). The peak fractions were pooled and concentrated to 15 mg/mL. The purity of LiLpxA was evaluated by SDS−PAGE, activity assay (*7*), and electrospray ionization mass spectrometry (*17*). The latter revealed a molecular weight of 28 165.0 (theoretical 28 165.1), indicating that the N-terminal methionine residue was deformylated.

Substrate Preparation and in Vitro Assay. The [α-^{32}P]-UDP-GlcNAc and [α-^{32}P]-UDP-GlcNAc3N substrates were prepared as previously described (*7*, *8*). LiLpxA-catalyzed conversion of [α-^{32}P]-UDP-GlcNAc3N to [α-^{32}P]-UDP-3-*O*-(*R*-3-hydroxylauroyl)-GlcNAc3N was monitored by thin-layer chromatography (TLC) on a silica gel 60 plate. A typical 10 μL reaction mixture contained 40 mM HEPES at pH 8.0, 1 mg/mL bovine serum albumin, 2.5 μM LpxC inhibitor CHIR-090 (*18*), 10 μM *R*-3-hydroxylauroyl-ACP (or varying concentrations of *R*-3-hydroxylauroyl-methylphosphopantetheine), and 10 μM [α-^{32}P]-UDP-GlcNAc3N. The reaction was started at 30 °C by the addition of an appropriate amount of enzyme. Product formation was monitored by spotting 1 μL samples at each time point onto a silica gel 60 TLC plate, which was developed with chloroform/methanol/water/acetic acid (25:15:4:2, v/v/v/v) and analyzed with a Storm 840 PhosphorImager (GE Healthcare, Chalfont, St. Giles, U.K.).

Synthesis of Carrier UDP-GlcNAc3N. In a 50 mL conical tube, 2.5 mL of 800 mM *N*-2-hydroxyethylpiperazine-*N*′-2-ethanesulfonic acid (HEPES) at pH 8, 20 mL of 1 M L-glutamate, 200 μL of 100 mM UDP-GlcNAc, 2 mL of 100 mM NAD^+, 2 mL of cell extract from *E. coli*/pCS355 (0.5 mg/mL) (*8*), and 13.3 mL of H_2O were mixed and incubated at 30 °C for 5 h. The reaction mixture was then filtered through a 0.2 μm syringe filter and loaded onto a Dionex (Sunnyvale, CA) CarboPac PA1 column (9 × 250 mm) in 5 mL increments at 2.0 mL/min using a Beckman System Gold HPLC. A gradient (120 mL) from 0.0 to 1.0 M ammonium acetate was used for each run; the product eluted between 300 and 400 mM ammonium acetate. The fractions containing the UDP-GlcNAc3N were combined and lyophilized to yield 1.4 mg of pure material. The exact mass of the product was confirmed by electrospray ionization mass spectrometry in the negative ion mode ($[M - H]^-$ observed at *m*/*z* 605.11).

LiLpxA Crystallization in the Absence of Ligand. Crystallization was performed using the hanging drop/vapor diffusion method. The hanging drop solution contained 2 μL of pure LiLpxA (15 mg/mL) and 2 μL of the reservoir solution. Searches for a crystallization condition were first carried out using Hampton crystal screens I and II (Aliso Viejo, CA). The conditions in this screen that yielded thin needle crystals contained 20% isopropanol, 1 M sodium citrate at pH 5.6, and 20% polyethylene glycol 4000. These crystals were optimized using a PEG/ion screen purchased from Hampton Research (Aliso Viejo, CA). Diffracting crystals, which appeared within 3−5 days and grew to ~0.3 mm in the largest dimension, were obtained from 20 to 25% (w/v) PEG 3350 and from 0.2 to 0.6 M diammonium citrate at pH 7.4. Crystals were flash-frozen in liquid nitrogen in a solution consisting of 30% (w/v) PEG 3350 and 0.2 M diammonium citrate. Crystals diffracted to 2.10 Å and belonged to space group *P*321 ($a = b = 109.15$ Å, $c = 117.12$ Å). The asymmetric unit contains three LpxA monomers.

Table 1: Data and Refinement Statistics for *L. interrogans* LpxA

	LiLpxA	LiLpxA/UDP-3-*N*-(*R*-3-hydroxylauroyl)-GlcNAc3N	LiLpxA/*R*-3-hydroxylauroyl-methylphosphopantetheine
source/detector	RU200/R-Axis IV	RU200/R-Axis IV	RU200/R-Axis IV
space group	*P*321	*P*321	*P*321
a, *b*, *c* (Å)	*a* = *b* = 109.15	*a* = *b* = 106.95	*a* = *b* = 108.16
	c = 117.12	*c* = 116.54	*c* = 116.87
wavelength (Å)	1.5415	1.5415	1.5415
resolution range[a] (Å)	26.3−2.10	46.3−2.10	24.8−2.12
last shell (Å)	2.15−2.10	2.15−2.10	2.18−2.12
unique reflections	44732	41810	41533
completeness (%) (last shell)	99.23 (99.7)	96.92 (99.7)	96.65 (98.96)
average I/σ (last shell)	12.8 (3.4)	30.6 (4.75)	14.8 (2.9)
redundancy (last shell)	7.1 (7.2)	3.5 (3.3)	5.7 (5.4)
R_{merge}[b] (%)	8.8	5.0	11.5
ligand atoms	0	6127	6604
protein atoms	5931	5968	6003
solvent atoms	379	315	473
rmsd from ideality			
bond lengths (Å)	0.009	0.011	0.009
bond angles (deg)	1.24	1.34	1.30
R value[c] (%)	21.7	21.6	19.8
R_{free}[c] (%)	26.0	25.8	25.8
all-atom clash score	5.6	9.6	7.4

[a] The resolution limit was defined as the highest resolution shell where the average I/σ_I was 2. [b] $R_{merge} = \sum_{hkl}\sum_i|I_{i(hkl)} - \langle I_{(hkl)}\rangle|/\sum_{hkl}\sum_i I_{(hkl)}$. [c] $R = \sum|F_o - F_c|/\sum F_o$; 5% of reflections were used to calculate R_{free}.

Preparation of the LiLpxA/R-3-Hydroxylauroyl-methylphosphopantetheine Complex. One LiLpxA crystal (~0.3 mm), obtained as described above, was transferred into a 2 μL drop at 18 °C containing an approximately 25-fold molar excess of *R*-3-hydroxylauroyl-methylphosphopantetheine over LiLpxA, along with 35% (w/v) PEG 3350 and 0.4 M diammonium citrate. After 20 min, the crystal was flash-frozen in liquid nitrogen.

Preparation of the LiLpxA/UDP-3-N-(R-3-Hydroxylauroyl)-GlcNAc3N Complex. One LiLpxA crystal (~0.3 mm), obtained as described above, was transferred into a 2 μL drop at 18 °C containing approximately a 25-fold molar excess of both *R*-3-hydroxylauroyl-methylphosphopantetheine and UDP-GlcNAc3N over LiLpxA, along with 35% (w/v) PEG 3350 and 0.4 M diammonium citrate. After 1 week at 18 °C, the crystal was flash-frozen in liquid nitrogen.

Data Collection, Structure Determination, and Refinement. Diffraction data were collected on a R-Axis IV image plate detector. Diffraction data were reduced and scaled using HKL2000 (*19*). Initial phases were obtained by molecular replacement using the program Phaser (*20*). *E. coli* LpxA (PDB code 1lxa) (*14*) was used as the model for molecular replacement of LiLpxA in the absence of ligand. This LiLpxA structure was used in turn as the starting model for the LiLpxA/*R*-3-hydroxylauroyl-methylphosphopantetheine and the LiLpxA/UDP-3-*N*-(*R*-3-hydroxylauroyl)-GlcNAc3N complexes. Iterative rounds of model building were performed using the programs O and Coot, with rounds of simulated annealing, energy minimization, and *B*-factor refinement in Refmac (*21*−*23*). The quality of the final model was assessed using MolProbity and PROCHECK (*24*, *25*). The figures were generated using PyMol (Delano Scientific LLC, South San Francisco, CA). Data and refinement statistics for all three structures are presented in Table 1.

RESULTS

Crystal Structure of LiLpxA in the Absence of Ligands. The LiLpxA protein (a single polypeptide of 259 amino acid residues) shows 41% identity and 59% similarity with EcLpxA over its full length (*3*, *26*). On the basis of the conservation of key active-site residues and mutagenesis studies (*7*, *11*), LiLpxA appears to function by a mechanism similar to that of EcLpxA (Schemes 1 and 2). To account for its distinct sugar nucleotide and acyl-chain selectivity (Figure 1), we crystallized LiLpxA and solved its structure at a resolution of 2.10 Å by molecular replacement, using free EcLpxA as the model (PDB code 1lxa) (*14*). The LiLpxA asymmetric unit contains three protein monomers (Figure 2) in the trigonal space group *P*321; in contrast, there is only one polypeptide chain in the EcLpxA asymmetric unit (Figure 2) in the space group $P2_13$ (*14*). The R_{work} and R_{free} values for LiLpxA converged at 0.22 and 0.26, respectively (Table 1). All 259 residues of LiLpxA were clearly resolved, with the exception of the methionine side chain at the N terminus.

The conformations of the three LiLpxA chains in the asymmetric unit (designated A, B, and C) are virtually the same (Figure 2A) and are each very similar to that of EcLpxA (*14*) (panels B and C of Figure 2). The N-terminal portion of the LiLpxA protein (residues 1−192) consists of a left-handed parallel β helix made up of 29 β sheets; 27 of these comprise 9 complete β-helical turns. At the fourth helical turn, a 13-residue loop is inserted, interrupting the β helix (lower arrow in Figure 2A). A loop of similar position and size is also present in EcLpxA (lower arrow in Figure 2B) (*14*). At the fifth turn of the LiLpxA β helix, a second smaller loop (consisting of six residues) is inserted (upper arrow in Figure 2A), but it is oriented differently than the corresponding loop in EcLpxA (upper arrow in Figure 2B and Figure 2C). The C-terminal portion of LiLpxA (residues 193−259) consists of four α helices (Figure 2A) and is similar to the corresponding region of EcLpxA (Figure 2B), albeit with a slightly different tilt (Figure 2C). Superposition of EcLpxA on chain A of LiLpxA yielded a rmsd of 0.899 Å for 213 C_α atom pairs (Figure 2C), as determined by PyMol (DeLano Scientific LLCs, South San Francisco, CA).

Scheme 2: Proposed Catalytic Mechanism of LiLpxA and Roles of Key Residues in Substrate Binding[a]

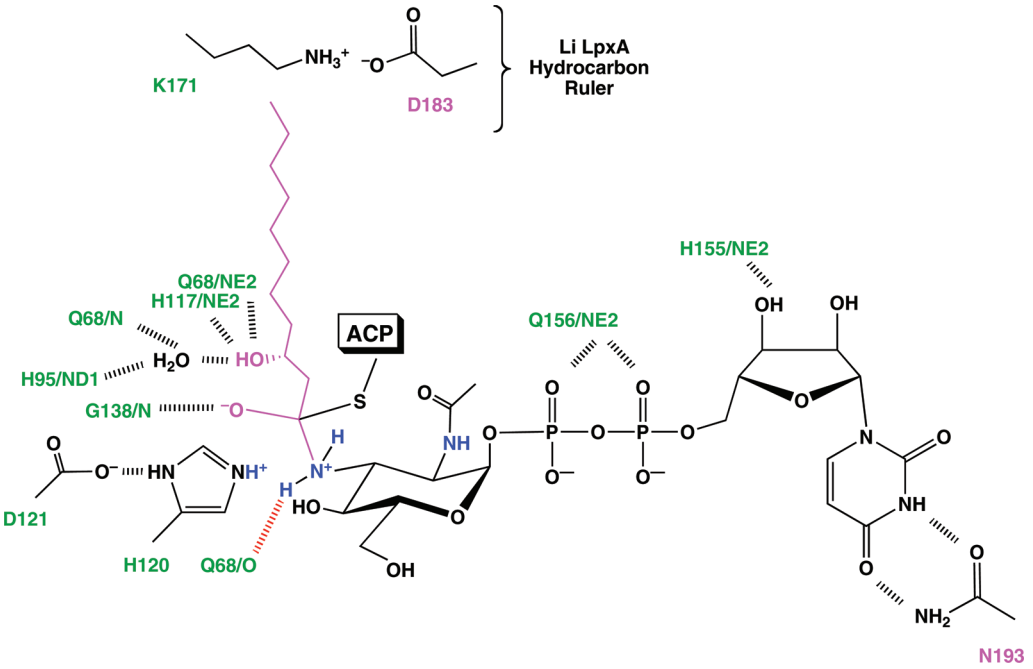

[a] The critical hydrogen bond formed between the 3-NH_2 group of the acceptor substrate and the backbone O atom of Q68 is shown in red.

Both EcLpxA and LiLpxA are homotrimers in aqueous solution, as judged by size-exclusion chromatography of the catalytically active enzyme. The arrangement of the subunits in the functional LiLpxA trimer (Figure 3A) is different than that in the asymmetric unit (Figure 2A). On the basis of an analysis of symmetry mates, we suggest that three A chains of the LiLpxA asymmetric unit rotated around a non-crystallographic 3-fold axis of symmetry constitute the biologically relevant trimer (Figure 3A); likewise, three B chains or three C chains but not mixtures of A, B, and C chains constitute a functional LiLpxA trimer (not shown). In both LiLpxA and EcLpxA, key active residues are positioned at the interfaces of adjacent subunits of the biological trimer (*12*) (Figure 3B). With the exception of the Q156 side chain (Figure 3B), the conserved residues of LiLpxA, which include H120, H117, H139, Q68, and N193 (not visible), align rather well with the corresponding EcLpxA residues (*11*, *12*, *14*) (Figure 3B). Given the overall structural similarity of EcLpxA versus LiLpxA, the explanation for the striking differences in the substrate selectivity of these enzymes was not immediately apparent from these results.

Activity of LiLpxA with R-3-Hydroxylauroyl-methylphosphopantetheine. Previous studies demonstrated that LiLpxA shows absolute selectivity for *R*-3-hydroxylauroyl-ACP over *R*-3-hydroxydecanoyl- or *R*-3-hydroxymyristoyl-ACP (*7*). However, synthetic *R*-3-hydroxylauroyl-methylphosphopantetheine (Avanti Polar Lipids) was an excellent alternative donor substrate for LiLpxA. At 50 μM *R*-3-hydroxylauroyl-methylphosphopantetheine and 10 μM UDP-GlcNAc3N, the specific activity of purified recombinant LiLpxA was 3×10^3 nmol min^{-1} mg^{-1}, comparable to what is seen with 10 μM *R*-3-hydroxylauroyl-ACP and 10 μM UDP-GlcNAc3N (Figure 4A) (*7*). The K_M for *R*-3-hydroxylauroyl-methylphosphopantetheine with 10 μM UDP-GlcNAc3N as the acceptor substrate is 4 μM (data not shown). Very little activity was seen with 200 μM *R*-3-hydroxylauroyl-coenzyme A (Figure 4B).

Structure of the LiLpxA/UDP-3-N-(R-3-Hydroxylauroyl)-GlcNAc3N Complex. Given that LiLpxA catalyzes a thermodynamically favorable reaction, a crystal of free LiLpxA was soaked with a 25-fold molar excess of both *R*-3-hydroxylauroyl-methylphosphopantetheine and UDP-GlcNAc3N, as described in the Materials and Methods. The presumed LpxA/UDP-3-*N*-(*R*-3-hydroxylauroyl)-GlcNAc3N complex diffracted to 2.10 Å and was solved by molecular replacement using free LiLpxA as the model. The asymmetric unit of the complex was again comprised of three polypeptide chains. Each chain bound one UDP-3-*N*-(*R*-3-hydroxylauroyl)-GlcNAc3N molecule (Figure 5). The electron density for the bound UDP-3-*N*-(*R*-3-hydroxylauroyl)-GlcNAc3N ligand was strong in each chain (expansions in Figure 5), especially in the region of the fatty acyl group. In chain B, the glucosamine ring was rotated relative to its positioning in chains A and C, but the electron density for the glucosamine ring in chain B was especially clear (Figure 5). However, the electron densities of the α- and β-phosphate moieties of the chain B ligand were somewhat weaker than the comparable densities in the other ligands. In chains A and C, the electron densities of the 5 and 6 hydroxyls of the GlcNAc3N moiety were weak but the GlcNAc3N orientation was similar to that of the GlcNAc unit in the EcLpxA/UDP-3-*O*-(*R*-3-hydroxymyristoyl)-GlcNAc complex (*12*) (see below).

Rotation around a 3-fold non-crystallographic axis of symmetry yields the biologically relevant homotrimer with a bound ligand, as shown for chain A in panels A and B of Figure 6, in which the green, pink, and blue subunits each consist of chain A of the asymmetric unit, with the corresponding ligands shown with space-filling atoms. In Figure 6A, the UDP-3-*N*-(*R*-3-hydroxylauroyl)-GlcNAc3N molecule in the foreground is positioned with its fatty acyl and GlcNAc3N moieties next to the green chain and its UDP moiety next to the adjacent pink chain. All three active sites of the biological LiLpxA trimer are presumed to be functional.

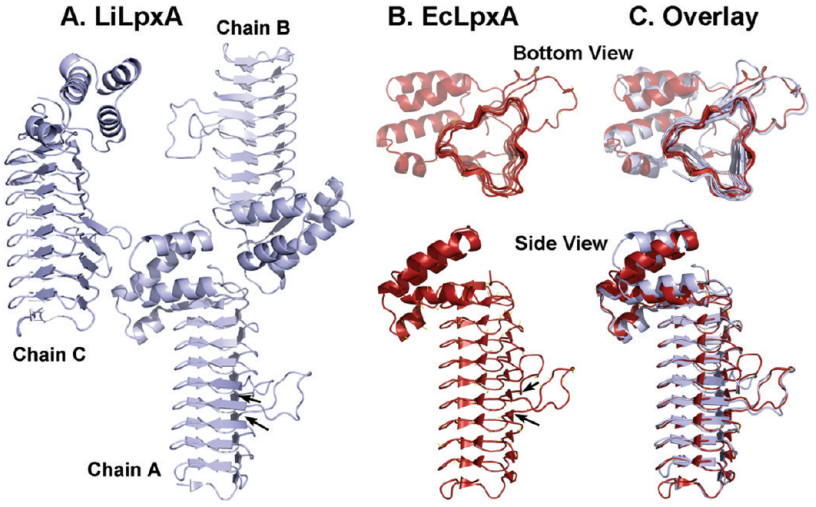

FIGURE 2: Asymmetric units and backbone structures of free LiLpxA versus EcLpxA. (A) There are three chains (light blue cartoon diagrams) in the LiLpxA asymmetric unit, each containing 259 residues. The N-terminal domain of each chain is folded into a left-handed parallel β helix. The C-terminal domain consists of four α helices. Black arrows in chain A indicate origins of loops inserted within the β-helix domain. (B) Bottom up and side views of the EcLpxA asymmetric unit (*14*), which consists of a single chain of 262 amino acids (red cartoon diagram). Loops of similar position and size (black arrows) to those seen in LiLpxA are present in the β-helix domain of EcLpxA. The second loop of LiLpxA is smaller and oriented differently than that of EcLpxA. (C) Superposition of EcLpxA (*14*) and chain A of LiLpxA.

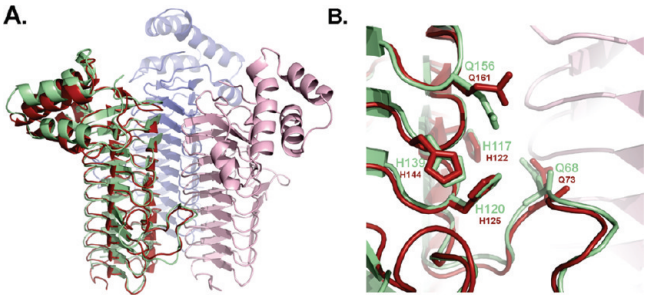

FIGURE 3: Structure of the biological LiLpxA homotrimer and position of active-site residues in the absence of ligands. (A) Side view of the free LiLpxA biological trimer (pale green, slate blue, and light pink cartoons), generated from chain A of the asymmetric unit. The EcLpxA monomer of its asymmetric unit (brick red) (*14*) is superimposed on one LiLpxA subunit for a comparison of the active-site region. (B) Close up view of superimposed active-site residues. LiLpxA H120 (corresponding to EcLpxA H125) is the catalytic base (Schemes 1 and 2). Q156 side chain of LiLpxA is displaced from that of the corresponding EcLpxA residue Q161. The backbone O atom of Q68 in LiLpxA is rotated relative to its counterpart in Q73 of EcLpxA.

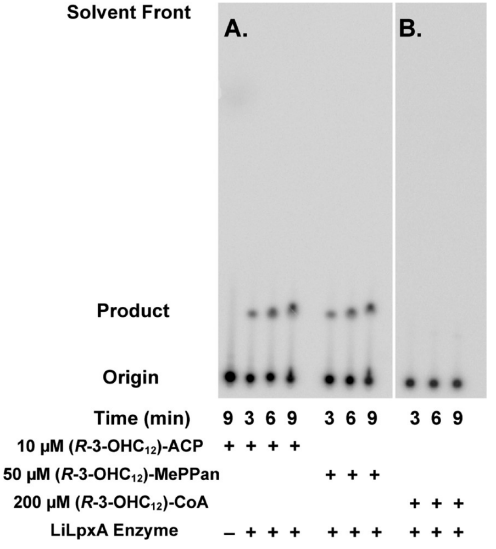

FIGURE 4: *R*-3-Hydroxylauroyl-methylphosphopantetheine as an acyl donor substrate for LiLpxA. In these assays, the concentration of UDP-GlcNAc3N was 10 μM. (A) Near equivalence of 10 μM *R*-3-hydroxylauroyl-ACP and 50 μM *R*-3-hydroxylauroyl-methylphosphopantetheine as donors. (B) Lack of activity of *R*-3-hydroxylauroyl-coenzyme A. Abbreviations: CoA, coenzyme A; MePPan, methyl-phosphopantetheine; *R*-3-OHC_{12}-, *R*-3-hydroxylauroyl-.

Polar Interactions between LiLpxA and Its Lipid Product. The hydrogen-bond network and polar groups of the biologically relevant LiLpxA trimer that interact with the UDP-3-*N*-(*R*-3-hydroxylauroyl)-GlcNAc3N product (Figure 6C) resemble those previously seen in the EcLpxA/UDP-3-*O*-(*R*-3-hydroxymyristoyl)-GlcNAc complex (PDB code 2qia) (*12*). The OH group of the *R*-3-hydroxylauroyl chain is within hydrogen-bonding distance of H117/NE2, Q68/NE2, and a highly ordered water molecule, also seen in the *E. coli* LpxA/product complex (Figure 6D) (*12*). The ordered water molecule participates in additional hydrogen bonds with H95/NE2 and the backbone N atom of Q68 of LiLpxA (Figure 6C). The carbonyl group of the *R*-3-hydroxylauroyl chain is within hydrogen-bonding distance of the backbone N atom of G138, which forms part of the putative oxyanion hole for the tetrahedral intermediate (Scheme 2). NE2 of H120, the presumed catalytic base, is within 3.4−3.9 Å (depending upon the chain of the LiLpxA asymmetric unit) of the 3-N atom of the GlcNAc3N moiety (Figure 6C). The side chain of R199 contributes a hydrogen bond to one oxygen atom on the α-phosphate group, while OD1 and ND2 of Q193 hydrogen bond the uracil residue. H155/NE2 hydrogen bonds the 4-OH group of the ribose ring, and NE2 of the Q156 side chain hydrogen bonds oxygen atoms on both the α and β phosphates (Figure 6C).

As shown in the EcLpxA/LiLpxA (chain A) product complex overlay (Figure 6D), the positioning of the aminosugar residues and *R*-3-OH moieties are virtually the same, as are the conformations of nearby side chains in the active site (*12*). A subtle difference is the orientation of the backbone carbonyl O atom of Q68 in LiLpxA (panels C and D of Figure 6), which is within hydrogen-bonding distance of the 3-N atom of the GlcNAc3N moiety in all three chains of the asymmetric unit: the actual distances are 2.8 Å in chain A (Figure 6C), 2.8 Å in chain

B (not shown), and 2.4 Å in chain C (not shown). This arrangement creates a favorable interaction for the binding and acylation of UDP-GlcNAc3N but would discriminate against the 3-OH group of UDP-GlcNAc by lone pair repulsion, possibly accounting for the remarkable UDP-GlcNAc3N selectivity of LiLpxA. In *E. coli*, the corresponding backbone O atom of Q73 is rotated by ~82° and is therefore too far removed (4.4 Å) to interact with the aminosugar moiety (Figure 6D) (*12*). Consequently, we suggest that EcLpxA can acylate either UDP-GlcNAc or UDP-GlcNAc3N with equal efficiency (*7*).

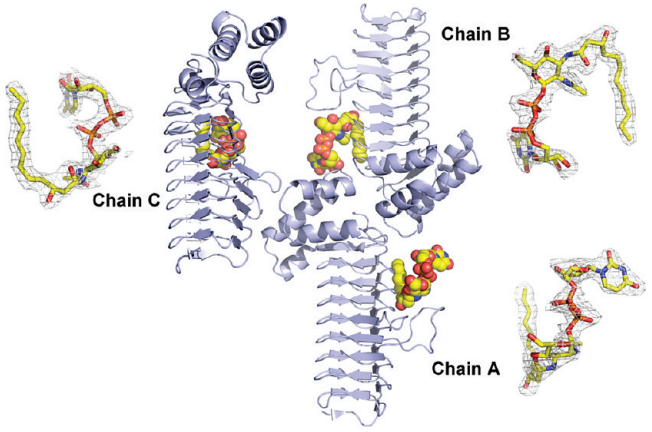

FIGURE 5: Asymmetric unit and ligand electron densities in the LiLpxA/UDP-3-*N*-(*R*-3-hydroxylauroyl)-GlcNAc3N complex. The UDP-3-*N*-(*R*-3-hydroxylauroyl)-GlcNAc3N ligands (space filling with yellow carbons) are shown together with their corresponding LiLpxA chains in the asymmetric unit (light blue cartoons). The actual electron density of each ligand (light gray mesh) is superimposed on an expanded stick model of UDP-3-*N*-(*R*-3-hydroxylauroyl)-GlcNAc3N in the best calculated conformation (carbons in yellow) next to its corresponding LiLpxA protein chain. The final $2F_o - F_c$ electron-density map is contoured at 1σ around each ligand.

Structure of the LiLpxA/R-3-Hydroxylauroyl-methylphosphopantetheine Complex. A crystal of LiLpxA was incubated with a 25-fold molar excess of *R*-3-hydroxylauroylmethylphosphopantetheine (Figure 7A), as described in the Materials and Methods. The LiLpxA/*R*-3-hydroxylauroylmethylphosphopantetheine complex diffracted to a resolution of 2.12 Å and was solved by molecular replacement with free LiLpxA as the model. Within each chain of the asymmetric unit, strong electron density was observed for the entire *R*-3-hydroxylauroyl moiety of the *R*-3-hydroxylauroyl-methylphosphopantetheine ligand (Figure 7B), the thioester-linked β-mercaptoethylamine unit, and the carbonyl group of the β-alanine residue (Figure 7B). In chain C of the asymmetric unit (Figure 7B), electron density was clearly seen for the entire β-alanine residue, albeit in two conformational states. Partial electron density suggestive of the locations of the pantoic acid carbonyl group and the methylphosphate moiety was visible in all three monomers (Figure 7B); this density was best modeled by assuming two conformational states. Whatever the exact conformation, the

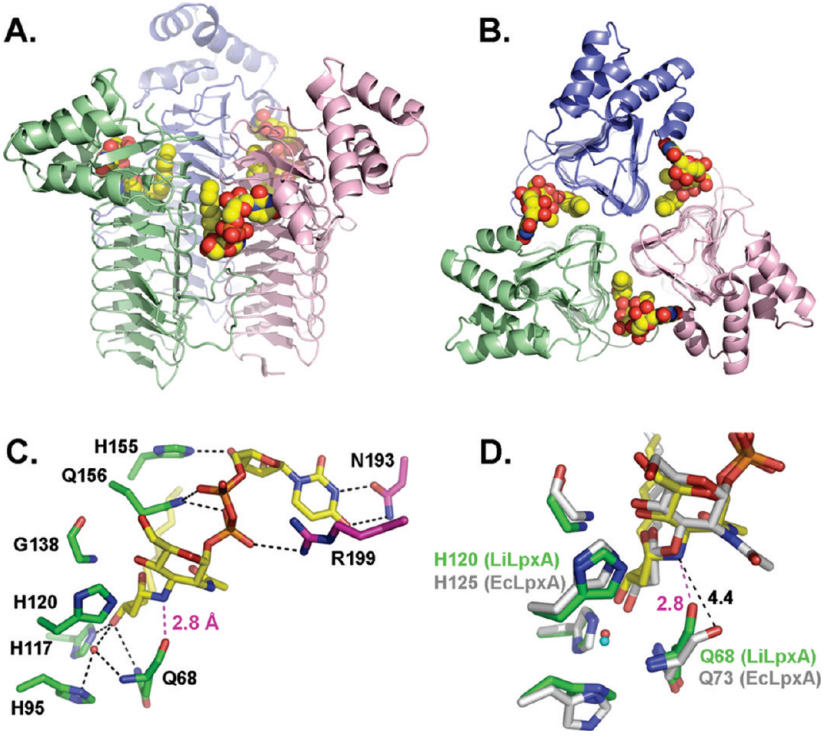

FIGURE 6: Position of the Q68 backbone O atom in the LiLpxA/UDP-3-*N*-(*R*-3-hydroxylauroyl)-GlcNAc3N complex. (A) Ribbon diagram of the biological LiLpxA homotrimer (generated from monomer A of the asymmetric unit) with a space-filling model of the bound product UDP-3-*N*-(*R*-3-hydroxylauroyl)-GlcNAc3N. The enzyme subunits of the biological homotrimer are colored in pale green, slate blue, and light pink. For UDP-3-*N*-(*R*-3-hydroxylauroyl)-GlcNAc3N, the carbon atoms are yellow, the oxygen atoms are red, the nitrogen atoms are blue, and the phosphorus atoms are orange. (B) Product complex viewed from the top down. (C) Close up of the positions of key active-site residues in LiLpxA in relation to bound UDP-3-*N*-(*R*-3-hydroxylauroyl)-GlcNAc3N. The color scheme for the ligand and protein is the same as above. Key hydrogen bonds are indicated with black dashes. The NE2 atom of H120 is the proposed catalytic base when catalysis proceeds in the forward direction (Scheme 2), and the backbone N atom of G138 is the proposed oxyanion hole. The ordered water molecule (red) that is hydrogen-bonded to the *R*-3-OH group of the product is seen in all three LiLpxA chains of the asymmetric unit (not shown). (D) Active-site residues in the LiLpxA/UDP-3-*N*-(*R*-3-hydroxylauroyl)-GlcNAc3N complex (chain A) versus the EcLpxA/UDP-3-*O*-(*R*-3-hydroxymyristoyl)-GlcNAc complex (*12*). The color scheme for LiLpxA and its ligand is the same as above. The color scheme for the *E. coli* protein and its ligand is also the same, except that all carbon atoms are gray. The ordered water molecule in the *E. coli* complex is cyan.

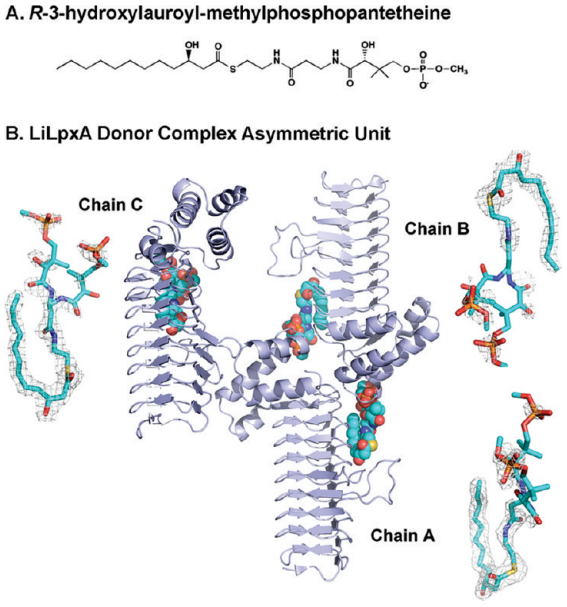

FIGURE 7: Asymmetric unit and ligand electron densities in the LiLpxA/*R*-3-hydroxylauroyl-methylphosphopantetheine complex. (A) Covalent structure of synthetic *R*-3-hydroxylauroyl-methylphosphopantetheine. (B) *R*-3-Hydroxylauroyl-methylphosphopantetheine ligands (space filling models with carbons in cyan) are shown together with their corresponding LiLpxA chains in the asymmetric unit (light blue cartoons). The actual electron density of each ligand (light gray mesh) is superimposed on an expanded stick model of the *R*-3-hydroxylauroyl-methylphosphopantetheine ligand in the best calculated conformations (carbons in cyan) next to its corresponding LiLpxA protein chain. The conformations and positions of the hydroxyacyl chains, the thioester linkages, and the β-mercaptoethylamine groups are very similar in each of the three ligands, and their electron densities are strong. The β-alanine, pantoic acids, and methyl phosphate groups are modeled in two conformations, and their electron densities are weak. The final $2F_o - F_c$ electron-density map is contoured at 1σ around each ligand. Thermal motions were analyzed for the donor but not the product complex using TLSMD (*41*).

acyl chain is folded, so that it remains in the proximity of and parallel to the extended pantetheine residue (Figure 7B).

As in the free LiLpxA structure (Figure 3A), the biologically relevant homotrimer with its bound donor substrate is formed by rotation around a non-crystallographic 3-fold axis of symmetry, as shown in Figure 8A for chain A. The two alternative conformations of the pantoic acid and methyl phosphate moieties are shown in Figure 8B. The *R*-3-hydroxylauroyl-methylphosphopantetheine interacts through a network of hydrogen bonds with the two adjacent subunits that constitute the LiLpxA active site. Many of these interactions are also observed in the LiLpxA/UDP-3-*N*-(*R*-3-hydroxylauroyl)-GlcNAc3N complex (Figure 6C). NE2 of H117, NE2 of Q68, and a single, well-defined water molecule directly hydrogen bond the *R*-3-OH group of the acyl chain (dashed black lines in Figure 8C). ND1 of H95 and the backbone N atom of Q68 interact with this same water molecule (Figure 8C), as seen in the product complex (dashed black lines in Figure 6C). OE1 of Q156 hydrogen bonds the N atom of the 2-mercaptoethylamine unit; an additional hydrogen bond is present between the side-chain OH group of S149 and the carbonyl group of the β-alanine moiety (Figure 8C).

Structural Basis for the Acyl-Chain Selectivity of LiLpxA. LiLpxA has no measurable activity *in vitro* with either *R*-3-hydroxymyristoyl-ACP or *R*-3-hydroxydecanoyl-ACP (*7*). This observation is explained by the shape of the acyl-chain binding site, which extends about 12 Å along a hydrophobic groove seen in both the LiLpxA/*R*-3-hydroxylauroyl-methylphosphopantetheine and the LiLpxA/UDP-3-*N*-(*R*-3-hydroxylauroyl)-GlcNAc3N complexes (panels C and D of Figure 8). This aliphatic cleft is created by residues A137, V135, A153, G150, and G168 (transparent spheres in Figure 8C) and is capped by the side chain of K171 (Figure 8C). K171 forms an ion pair with D183 from the opposing subunit (transparent spheres in Figure 8C), preventing the binding of longer acyl chains to LiLpxA. The terminal methyl groups of both the UDP-3-*N*-(*R*-3-hydroxylauroyl)-GlcNAc3N and the *R*-3-hydroxylauroyl-methylphosphopantetheine are situated ~3.8 Å from the C_ε atom of K171 and superimpose very well on each other (Figure 8D). From the structural analysis, it appears that K171 functions as the primary hydrocarbon ruler, limiting the length of the acyl chain used by LiLpxA. In EcLpxA, K171 is replaced by a G residue. Attempts to replace K171 with G in LiLpxA were unsuccessful (not shown); the resulting mutant protein was unstable, perhaps because the ion pair with D183 can no longer be formed (Figure 8C). As shown in Figure 8D, conformation 1 of the *R*-3-hydroxylauroyl-methylphosphopantetheine donor substrate might be preferred during catalysis, because there is less steric clash with the UDP moiety. More crystal structures, especially of LiLpxA with its physiologically relevant *R*-3-hydroxylauroyl-ACP donor substrate, will be required to resolve this issue.

DISCUSSION

Some Gram-negative bacteria, including the pathogen *L. interrogans*, synthesize lipid A disaccharides, in which both GlcN residues are replaced with the analogue GlcN3N (Figure 1) (*5*, *27*). These bacteria nevertheless encode orthologues of all of the *E. coli lpx* genes (*27*, *28*) responsible for lipid A assembly, indicating that the enzymatic pathway for lipid A biosynthesis is conserved. Previous studies from our laboratory have shown that the GlcN3N unit is generated from UDP-GlcNAc by two enzymes, designated GnnA and GnnB (Figure 1), present in all bacteria that make GlcN3N-containing lipid A (*8*).

The first step of lipid A biosynthesis in *E. coli* is catalyzed by LpxA, which transfers the *R*-3-hydroxymyristate moiety from *R*-3-hyrdoxymyristoyl-ACP to the GlcNAc 3-OH position of UDP-GlcNAc (Figure 1) (*9*, *29*). EcLpxA prefers *R*-3-hydroxymyristoyl-ACP over *R*-3-hydroxylauroyl-ACP or *R*-3-hydroxypalmitoyl-ACP by a factor of ~50 (*9*), consistent with the structure of *E. coli* lipid A (Figure 1). Furthermore, EcLpxA does not use fatty acyl coenzyme A derivatives as donor substrates, and it has an absolute requirement for acyl chains containing the *R*-3-OH group (*9*−*11*). *In vitro*, EcLpxA can use UDP-GlcNAc3N as an acceptor substrate at about the same rate as UDP-GlcNAc (*7*), but wild-type *E. coli* does not encode GnnA and GnnB and therefore does not make UDP-GlcNAc3N. Heterologous expression of the *Acidithiobacillus ferrooxidans gnnA* and *gnnB* genes in *E. coli* results in the production of a "mixed" lipid A moiety, in which about one-third of the GlcN units are replaced with GlcN3N (*7*).

LiLpxA, which shows 41% identity and 59% similarity to EcLpxA over its full length (*7*), displays a remarkable selectivity for *R*-3-hydroxylauroyl-ACP and UDP-GlcNAc3N, consistent with the structure of *L. interrogans* lipid A (Figure 1) (*6*, *7*). To determine how LiLpxA discriminates against UDP-GlcNAc and selects for *R*-3-hydroxylauroyl chains, we solved its crystal structure at a resolution of 2.10 Å (Table 1). The β-helical domain and overall architecture of LiLpxA are very similar to EcLpxA. Superposition of the two enzymes (Figure 3) shows only minimal

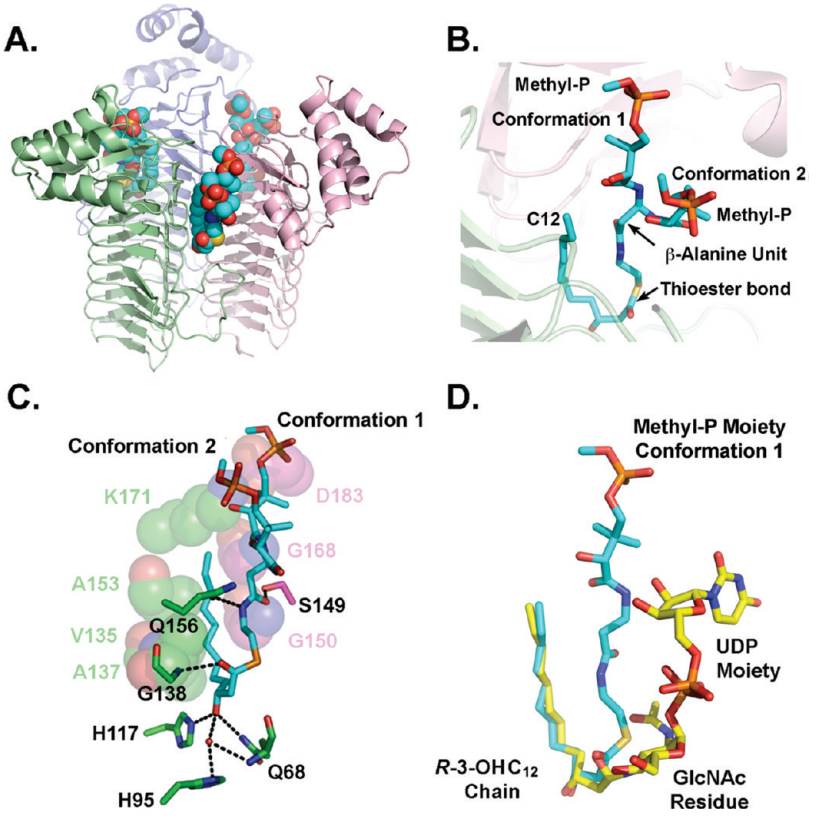

FIGURE 8: Position of the *R*-3-hydroxylauroyl-methylphosphopantetheine donor substrate at the LiLpxA active site. (A) Ribbon diagram of the LiLpxA biological homotrimer with a space-filling model of the bound donor substrate *R*-3-hydroxylauroyl-methylphosphopantetheine, modeled in two conformations. The subunits of the biological LiLpxA homotrimer (generated from chain A of the asymmetric unit) are colored as in Figure 6A. The atoms of *R*-3-hydroxylauroyl-methylphosphopantetheine are colored as follows: carbon, cyan; oxygen, red; nitrogen, blue; sulfur, yellow−orange; and phosphorus, orange. (B) Close-up view of the alternative conformations of the *R*-3-hydroxylauroyl-methylphosphopantetheine ligand. Abbreviation: Methyl-P, methyl phosphate residue. (C) Positions of key active-site residues in LiLpxA in relation to bound *R*-3-hydroxylauroyl-methylphosphopantetheine. The color scheme for the ligand is the same as above. The green and magenta carbons of LiLpxA side chains correspond to the similarly colored ribbons in A to distinguish the subunits of the biological LiLpxA trimer. Key hydrogen bonds are indicated with black dashes. The backbone N atom of G138 is the proposed oxyanion hole. The ordered water molecule (red) that is hydrogen-bonded to both the *R*-3-OH group is seen in all three LiLpxA monomers of the asymmetric unit (not shown) and is the same as in the product complex. The hydrophobic cleft that defines the acyl-chain binding site is highlighted by the transparent spheres. (D) Superposition of conformation 1 of the bound donor substrate (cyan carbons) and the bound product (yellow carbons), each associated with chain A of their respective asymmetric units. Abbreviations: Methyl-P, methyl phosphate residue; *R*-3-OHC_{12}-, *R*-3-hydroxylauroyl-.

changes in the orientations of conserved side chains involved in substrate binding (H117, H139, N193, and Q68) and catalysis (H120). Previous mutagenesis studies had already demonstrated the importance of H120 for LiLpxA activity (Figure 3) (*7*), which is the counterpart of the catalytic base H125 in EcLpxA (Scheme 1). A slight difference in the orientation of the Q156 side chain is apparent (Figure 3B), but its significance is not clear from the structure. Another difference between the two structures is the replacement of K76 in EcLpxA (Scheme 1) with G. When G71 of LiLpxA (the corresponding residue) was changed to K, the mutant enzyme still did not use UDP-GlcNAc; however, it remained fully active and selective for UDP-GlcNAc3N (data not shown). In summary, the structure of free LilpxA did not reveal the mechanistic basis for its UDP-GlcNAc3N selectivity.

We previously reported the structures of EcLpxA complexes with UDP-3-*O*-(*R*-3-hydroxydecanoyl)-GlcNAc and UDP-3-*O*-(*R*-3-hydroxymyristoyl)-GlcNAc, providing direct evidence for the side-chain interactions shown in Scheme 1 (*12*). The corresponding crystallographic analysis of LiLpxA containing its bound product was greatly facilitated by our discovery that LiLpxA uses the synthetic substrate analogue *R*-3-hydroxylauroyl-methylphosphopantetheine almost as efficiently as *R*-3-hydroxylauroyl-ACP (Figure 4A); however, *R*-3-hydroxylauroyl-coenzyme A was not a substrate (Figure 4B). LiLpxA crystals acylated UDP-GlcNAc3N efficiently, when incubated with a 25-fold molar excess of UDP-GlcNAc3N and *R*-3-hydroxylauroyl-methylphosphopantetheine over LiLpxA. The resulting complex diffracted to 2.10 Å (Table 1). Each chain of the asymmetric unit contained a bound product ligand with strong electron density (Figure 5).

As highlighted in the overlay of the product complexes of EcLpxA and LiLpxA (Figure 6D), the backbone carbonyl group of Q68 in LiLpxA is positioned to hydrogen bond the 3-NH_2 group of the UDP-GlcNAc3N substrate. However, with the GlcNAc 3-OH group of UDP-GlcNAc, this interaction would be unfavorable in the tetrahedral intermediate (Schemes 1 and 2) because of lone pair electron repulsion. In EcLpxA (*12*, *14*), the backbone carbonyl oxygen of the corresponding Q73 residue is rotated by ~82° compared to LiLpxA and is therefore too far removed to interact with either substrate (Figure 6D). Consequently, EcLpxA cannot discriminate between UDP-GlcNAc and UDP-GlcNAc3N and uses both with equal efficiency (*7*). Whether or not the hydrogen bonding of the Q68 carbonyl group to the 3-NH_2 moiety of the donor substrate by itself accounts for the sugar nucleotide selectivity of LiLpxA will require

additional, higher resolution crystal structures of LiLpxA/substrate complexes and a full evaluation of their hydrogen-bond inventories, including bound water molecules.

The manner in which LiLpxA discriminates against UDP-GlcNAc is reminiscent of the mechanism of vancomycin resistance in Gram-positive bacteria (*31*). These organisms can mutate their pathway for cell-wall peptide biosynthesis to terminate with D-Ala-D-lactate in place of the usual D-Ala-D-Ala moiety (*31*). Replacement of the amide linkage between the two D-Ala residues with an ester results in the loss of a critical hydrogen bond between vancomycin and the D-Ala-D-Ala moiety, accounting for a 1000-fold decrease in antibiotic potency (*31*−*33*). A synthetic model study of this phenomenon determined that the introduction of lone pair repulsion also contributed significantly to the increased resistance to vancomycin (*34*).

No previous structures have defined the position of the thioester bond of an acyl donor substrate for LpxA (panels C and D of Figure 8). Structures of several acyl-ACPs have been published (*35*, *36*), and modeling studies have suggested the location of the ACP docking site on EcLpxA (*37*). Superposition of the LiLpxA/*R*-3-hydroxylauroyl-methylphosphopantetheine and LiLpxA/UDP-3-*N*-(*R*-3-hydroxylauroyl)-GlcNAc3N ligands (Figure 8D) places the thioester bond in a reasonable position for nucleophilic attack by the 3-NH_2 group of UDP-GlcNAc3N, when the reaction proceeds in the forward direction. Only conformation 1 of the *R*-3-hydroxylauroyl-methylphosphopantetheine ligand is shown in Figure 8D, but the thioester linkage is in the same place in conformation 2 (Figure 8C).

K171 appears to be the "hydrocarbon ruler" of LiLpxA that accounts for its strict *R*-3-hydroxylauroyl selectivity (transparent space-filling side chain in Figure 8C). The terminal methyl groups of the ligand acyl chains in both the substrate and product complexes are located within 3.8 Å of the C_ε atom of K171 (panels C and D of Figure 8). Longer acyl chains would cause steric hindrance, while shorter acyl chains would result in decreased binding energy. The crystal structure of the EcLpxA/UDP-3-*O*-(*R*-3-hydroxymyristoyl)-GlcNAc complex identified its "hydrocarbon ruler" as the side chain of H191, preventing the binding of longer chains (*12*). Furthermore, the G173M mutation converts EcLpxA into a C10-specific enzyme by reducing the size of the acyl-chain binding cavity (*10*). High-resolution structures of LpxA orthologues with longer (*38*) or shorter acyl-chain selectivity may provide additional insights into the acyl-chain selection mechanism.

The information presented above may be useful for the development of inhibitors specific for LpxA. Peptide 920 (*39*, *40*), which consists of 15 amino acid residues, is a potent inhibitor of EcLpxA but not of LiLpxA (data not shown). Superposition of the LiLpxA structure on that of the EcLpxA/peptide 920 complex revealed steric clashes of several peptide 920 side chains with certain LiLpxA residues (not shown). However, the backbone of peptide 920 fits reasonably well into the LiLpxA active site. It may therefore be possible to design peptides or peptide analogues that specifically target LiLpxA.

ACKNOWLEDGMENT

We thank Dr. James Phillips and the late Dr. Joshua J. Warren for helpful advice with the crystallography, refinement issues, and molecular modeling. We thank Dr. Pei Zhou, Dr. David Six, Dr. Sang Hoon Joo, and Louis Metzger for their critical reading of the manuscript. We are especially grateful to Dr. Sang Hoon Joo for carefully annotating the PDB files.

REFERENCES

(1) Levett, P. N. (2001) Leptospirosis. *Clin. Microbiol. Rev. 14*, 296–326.
(2) Farr, R. W. (1995) Leptospirosis. *Clin. Infect. Dis. 21*, 1–6.
(3) Ren, S. X., Fu, G., Jiang, X. G., Zeng, R., Miao, Y. G., Xu, H., Zhang, Y. X., Xiong, H., Lu, G., Lu, L. F., Jiang, H. Q., Jia, J., Tu, Y. F., Jiang, J. X., Gu, W. Y., Zhang, Y. Q., Cai, Z., Sheng, H. H., Yin, H. F., Zhang, Y., Zhu, G. F., Wan, M., Huang, H. L., Qian, Z., Wang, S. Y., Ma, W., Yao, Z. J., Shen, Y., Qiang, B. Q., Xia, Q. C., Guo, X. K., Danchin, A., Saint Girons, I., Somerville, R. L., Wen, Y. M., Shi, M. H., Chen, Z., Xu, J. G., and Zhao, G. P. (2003) Unique physiological and pathogenic features of *Leptospira interrogans* revealed by whole-genome sequencing. *Nature 422*, 888–893.
(4) Bulach, D. M., Kalambaheti, T., de la Pena-Moctezuma, A., and Adler, B. (2000) Lipopolysaccharide biosynthesis in *Leptospira*. *J. Mol. Microbiol. Biotechnol. 2*, 375–380.
(5) Weckesser, J., and Mayer, H. (1988) Different lipid A types in lipopolysaccharides of phototrophic and related non-phototrophic bacteria. *FEMS Microbiol. Rev. 4*, 143–153.
(6) Que-Gewirth, N. L. S., Ribeiro, A. A., Kalb, S. R., Cotter, R. J., Bulach, D. M., Adler, B., Saint Girons, I., Werts, C., and Raetz, C. R. H. (2004) A methylated 1-phosphate group and four amide-linked acyl chains in *Leptospira interrogans* lipid A. The membrane anchor of an unusual lipopolysaccharide that activates TLR2. *J. Biol. Chem. 279*, 25420–25429.
(7) Sweet, C. R., Williams, A. H., Karbarz, M. J., Werts, C., Kalb, S. R., Cotter, R. J., and Raetz, C. R. H. (2004) Enzymatic synthesis of lipid A molecules with four amide-linked acyl chains. LpxA acyltransferases selective for a new analogue of UDP-*N*-acetylglucosamine in which an amine replaces the 3′′-hydroxyl group. *J. Biol. Chem. 279*, 25411–25419.
(8) Sweet, C. R., Ribeiro, A. A., and Raetz, C. R. H. (2004) Oxidation and transamination of the 3′′-position of UDP-*N*-acetylglucosamine by enzymes from *Acidithiobacillus ferrooxidans*. Role in the formation of lipid A molecules with four amide-linked acyl chains. *J. Biol. Chem. 279*, 25400–25410.
(9) Anderson, M. S., and Raetz, C. R. H. (1987) Biosynthesis of lipid A precursors in *Escherichia coli*: A cytoplasmic acyltransferase that converts UDP-*N*-acetylglucosamine to UDP-3-*O*-(*R*-3-hydroxymyristoyl)-*N*-acetylglucosamine. *J. Biol. Chem. 262*, 5159–5169.
(10) Wyckoff, T. J. O., Lin, S., Cotter, R. J., Dotson, G. D., and Raetz, C. R. H. (1998) Hydrocarbon rulers in UDP-*N*-acetylglucosamine acyltransferases. *J. Biol. Chem. 273*, 32369–32372.
(11) Wyckoff, T. J., and Raetz, C. R. H. (1999) The active site of *Escherichia coli* UDP-*N*-acetylglucosamine acyltransferase. Chemical modification and site-directed mutagenesis. *J. Biol. Chem. 274*, 27047–27055.
(12) Williams, A. H., and Raetz, C. R. H. (2007) Structural basis for the acyl chain selectivity and mechanism of UDP-*N*-acetylglucosamine acyltransferase. *Proc. Natl. Acad. Sci. U.S.A. 104*, 13543–13550.
(13) Anderson, M. S., Bull, H. S., Galloway, S. M., Kelly, T. M., Mohan, S., Radika, K., and Raetz, C. R. H. (1993) UDP-*N*-acetylglucosamine acyltransferase of *Escherichia coli*: The first step of endotoxin biosynthesis is thermodynamically unfavorable. *J. Biol. Chem. 268*, 19858–19865.
(14) Raetz, C. R. H., and Roderick, S. L. (1995) A left-handed parallel ss helix in the structure of UDP-*N*-acetylglucosamine acyltransferase. *Science 270*, 997–1000.
(15) Miller, J. R. (1972) Experiments in Molecular Genetics , Cold Spring Harbor Laboratory, Cold Spring Harbor, NY.
(16) Sambrook, J. G., and Russell, D. W. (2001) Molecular Cloning: A Laboratory Manual , 3rd ed., Cold Spring Harbor Laboratory, Cold Spring Harbor, NY.
(17) McClerren, A. L., Zhou, P., Guan, Z., Raetz, C. R. H., and Rudolph, J. (2005) Kinetic analysis of the zinc-dependent deacetylase in the lipid A biosynthetic pathway. *Biochemistry 44*, 1106–1113.
(18) McClerren, A. L., Endsley, S., Bowman, J. L., Andersen, N. H., Guan, Z., Rudolph, J., and Raetz, C. R. H. (2005) A slow, tight-binding inhibitor of the zinc-dependent deacetylase LpxC of lipid A biosynthesis with antibiotic activity comparable to ciprofloxacin. *Biochemistry 44*, 16574–16583.
(19) Otwinowski, Z., and Minor, W. (1997) Processing of X-ray diffraction data collected in oscillation mode. *Methods Enzymol. 276*, 307–326.
(20) Storoni, L. C., McCoy, A. J., and Read, R. J. (2004) Likelihood-enhanced fast rotation functions. *Acta Crystallogr., Sect. D: Biol. Crystallogr. 60*, 432–438.
(21) Jones, T. A., and Kjeldgaard, M. (1993) O, version 5.9, the manual.
(22) Emsley, P., and Cowtan, K. (2004) Coot: Model-building tools for molecular graphics. *Acta Crystallogr., Sect. D: Biol. Crystallogr. 60*, 2126–2132.

(23) Murshudov, G. N., Vagin, A. A., and Dodson, E. J. (1997) Refinement of macromolecular structures by the maximum-likelihood method. *Acta Crystallogr., Sect. D: Biol. Crystallogr. 53*, 240–255.
(24) Lovell, S. C., Davis, I. W., Arendall, W. B.III, de Bakker, P. I., Word, J. M., Prisant, M. G., Richardson, J. S., and Richardson, D. C. (2003) Structure validation by C_α geometry: ϕ,ψ and C_β deviation. *Proteins 50*, 437–450.
(25) Davis, I. W., Murray, L. W., Richardson, J. S., and Richardson, D. C. (2004) MOLPROBITY: Structure validation and all-atom contact analysis for nucleic acids and their complexes. *Nucleic Acids Res. 32*, W615–W619.
(26) Blattner, F. R., Plunkett, G., Bloch, C. A., Perna, N. T., Burland, V., Riley, M., Collado-Vides, J., Glasner, J. D., Rode, C. K., Mayhew, G. F., Gregor, J., Davis, N. W., Kirkpatrick, H. A., Goeden, M. A., Rose, D. J., Mau, B., and Shao, Y. (1997) The complete genome sequence of *Escherichia coli* K-12. *Science 277*, 1453–1474.
(27) Raetz, C. R. H., Reynolds, C. M., Trent, M. S., and Bishop, R. E. (2007) Lipid A modification systems in Gram-negative bacteria. *Annu. Rev. Biochem. 76*, 295–329.
(28) Raetz, C. R. H., and Whitfield, C. (2002) Lipopolysaccharide endotoxins. *Annu. Rev. Biochem. 71*, 635–700.
(29) Coleman, J., and Raetz, C. R. H. (1988) First committed step of lipid A biosynthesis in *Escherichia coli*: Sequence of the *lpxA* gene. *J. Bacteriol. 170*, 1268–1274.
(30) Bartling, C. M., and Raetz, C. R. H. (2008) Steady-state kinetics and mechanism of LpxD, the *N*-acyltransferase of lipid A biosynthesis. *Biochemistry 47*, 5290–5302.
(31) Walsh, C. T. (1993) Vancomycin resistance: Decoding the molecular logic. *Science 261*, 308–309.
(32) Williams, D. H., and Bardsley, B. (1999) The vancomycin group of antibiotics and the fight against resistant bacteria. *Angew. Chem., Int. Ed. Engl. 38*, 1172–1193.
(33) Kuzin, A. P., Sun, T., Jorczak-Baillass, J., Healy, V. L., Walsh, C. T., and Knox, J. R. (2000) Enzymes of vancomycin resistance: The structure of D-alanine-D-lactate ligase of naturally resistant *Leuconostoc mesenteroides*. *Structure 8*, 463–470.
(34) McComas, C. C., Crowley, B. M., and Boger, D. L. (2003) Partitioning the loss in vancomycin binding affinity for D-Ala-D-Lac into lost H-bond and repulsive lone pair contributions. *J. Am. Chem. Soc. 125*, 9314–9315.
(35) Roujeinikova, A., Baldock, C., Simon, W. J., Gilroy, J., Baker, P. J., Stuitje, A. R., Rice, D. W., Slabas, A. R., and Rafferty, J. B. (2002) X-ray crystallographic studies on butyryl-ACP reveal flexibility of the structure around a putative acyl chain binding site. *Structure 10*, 825–835.
(36) Roujeinikova, A., Simon, W. J., Gilroy, J., Rice, D. W., Rafferty, J. B., and Slabas, A. R. (2007) Structural studies of fatty acyl-(acyl carrier protein) thioesters reveal a hydrophobic binding cavity that can expand to fit longer substrates. *J. Mol. Biol. 365*, 135–145.
(37) Jain, N. U., Wyckoff, T. J., Raetz, C. R. H., and Prestegard, J. H. (2004) Rapid analysis of large protein−protein complexes using NMR-derived orientational constraints: The 95 kDa complex of LpxA with acyl carrier protein. *J. Mol. Biol. 343*, 1379–1389.
(38) Lee, B. I., and Suh, S. W. (2003) Crystal structure of UDP-*N*-acetylglucosamine acyltransferase from *Helicobacter pylori*. *Proteins 53*, 772–774.
(39) Benson, R. E., Gottlin, E. B., Christensen, D. J., and Hamilton, P. T. (2003) Intracellular expression of peptide fusions for demonstration of protein essentiality in bacteria. *Antimicrob. Agents Chemother. 47*, 2875–2881.
(40) Williams, A. H., Immormino, R. M., Gewirth, D. T., and Raetz, C. R. H. (2006) Structure of UDP-*N*-acetylglucosamine acyltransferase with a bound antibacterial pentadecapeptide. *Proc. Natl. Acad. Sci. U.S.A. 103*, 10877–10882.
(41) Painter, J., and Merritt, E. A. (2006) Optimal description of a protein structure in terms of multiple groups undergoing TLS motion. *Acta Crystallogr., Sect. D: Biol. Crystallogr. 62*, 439–450.